FFI RAPPORT

Tensile tests of Wolfram Carbide hard cores

Frøyland Øyvind, Moxnes John F

FFI/RAPPORT-2006/03865

FFI-V/1026/04

Tensile tests of Wolfram Carbide hard cores

Frøyland Øyvind, Moxnes John F

FORSVARETS FORSKNINGSINSTITUTT (FFI)
Norwegian Defence Research Establishment

P O BOX 25
N0-2027 KJELLER, NORWAY
REPORT DOCUMENTATION PAGE

1) PUBL/REPORT NUMBER	2) SECURITY CLASSIFICATION	3) NUMBER OF PAGES
FFI/RAPPORT-2006/03865	UNCLASSIFIED	
1a) PROJECT REFERENCE	2a) DECLASSIFICATION/DOWNGRADING SCHEDULE	29
FFI-V/1026/04	-	

4) TITLE

Tensile tests of Wolfram Carbide hard cores

5) NAMES OF AUTHOR(S) IN FULL (surname first)

Frøyland Øyvind , Moxnes John F.

6) DISTRIBUTION STATEMENT

Approved for public release. Distribution unlimited. (Offentlig tilgjengelig)

7) INDEXING TERMS

IN ENGLISH:		IN NORWEGIAN:	
a)	Wolfram Carbide	a)	Wolframkarbid
b)	Hard cores	b)	Hardkjerner
c)	Tensile tests	c)	Strekktester
d)	Constitutive equations	d)	Basislikninger
e)	Experimental	e)	Eksperimentell

THESAURUS REFERENCE:

8) ABSTRACT

In this report an experimental study of the tensile strength of different hard cores of Wolfram Carbide was performed. A bending test was constructed for the study. We show that the tensile strength and strain is smaller than the compressive strength and strain.

By comparing the measured longitudinal and transversal strain, we show that assuming a state of simple tension at the lower surface of the hardcore during bending is a good approximation.

The Young's modulus is somewhat larger in tension than in compression. The tensile stress as a function of the strain somewhat follows the compression curves in the linear compressive stress- strain region. The lack of non-linearity compared to the compressive curve we believed to be related to the mechanical properties of Cobalt that acts as glue for the Wolfram Carbide particles that constitute the hardcore.

9) DATE	AUTHORIZED BY	POSITION
	This page only	
2007-06-08	Bjarne Haugstad	Director of Research

CONTENTS

Tensile tests of wolfram carbide

1 INTRODUCTION

Good material models are necessary requisites for applying computer simulations. To achieve predictably of these mathematical material models, they are usually tuned to experimental data from tests very different from the actual set up for a specific computer simulation. The reason for this procedure is that most material models have many free parameters, which always can be tuned to match a specific problem. By establishing material data from one type of test, and achieving good simulation results for very different types of tests, good credibility of material models are achieved.

Nammo Raufoss AS is the inventor of the Multipurpose (MP) ammunition concept. The MP technology was developed during the end of the 60s and the first series production started in the beginning of the 70s. Still the product is of great importance for the company. Large volumes of ammunition are delivered for the armed forces around the world and in Norway.

The hard core of the 25 mm MP projectile consists of a high-density wolfram carbide-cobalt (WC-Co) hardmetal. The penetration capabilities of the hardmetal core are strongly dependent of the material properties. Of special interest is the tensile and compressive strength of this hard metal, which is very attractive. The greatest limitation when using hard metal materials is the in general low ductility in comparison to for instance some steel materials. Thus when the stresses reach the fracture stress the low ductility leads to a fast decrease in the strength due to damage. For steel materials the strength stays high for much larger plastic strains due to the, in general, larger ductility.

During penetration at approximately 90 degrees NATO the compressive strength of the hardmetal core is the most important quantity, while during exit of a target or during oblique impact the tensile strength is more important. In general the best penetrator is one that does not fracture during impact and penetration, but fractures during exit. When the hardmetal core fractures during exit the number of fragments increases and in general enhances damage to the structure behind the armour. During exit the tensile strength is the most important material parameter due to negative pressures that is developed in the hardcore.

We have preciously studied the compressive strength of WC-Co hardmetal [1-2]. In this report we study the tensile properties by using a bending test. The bending test is more reliable than a simple tension test. During simple tension the results can be significantly affected by the grip on the specimen during tension. On the other hand, the theoretical calculation becomes more complex for a bending test.

We have constructed a new experimental design for our study. The design is not according to the ISO standard (3327-1982) but we show that the experimental results match the theory [3-4].

2   THE EXPERIMENTAL SETUP FOR THE BENDING TEST

We have used two different setups for the bending test since two different hardcores with different diameters have been used for the study. Figure 2.1 shows the setup for the hardcore of 7 mm in diameter.
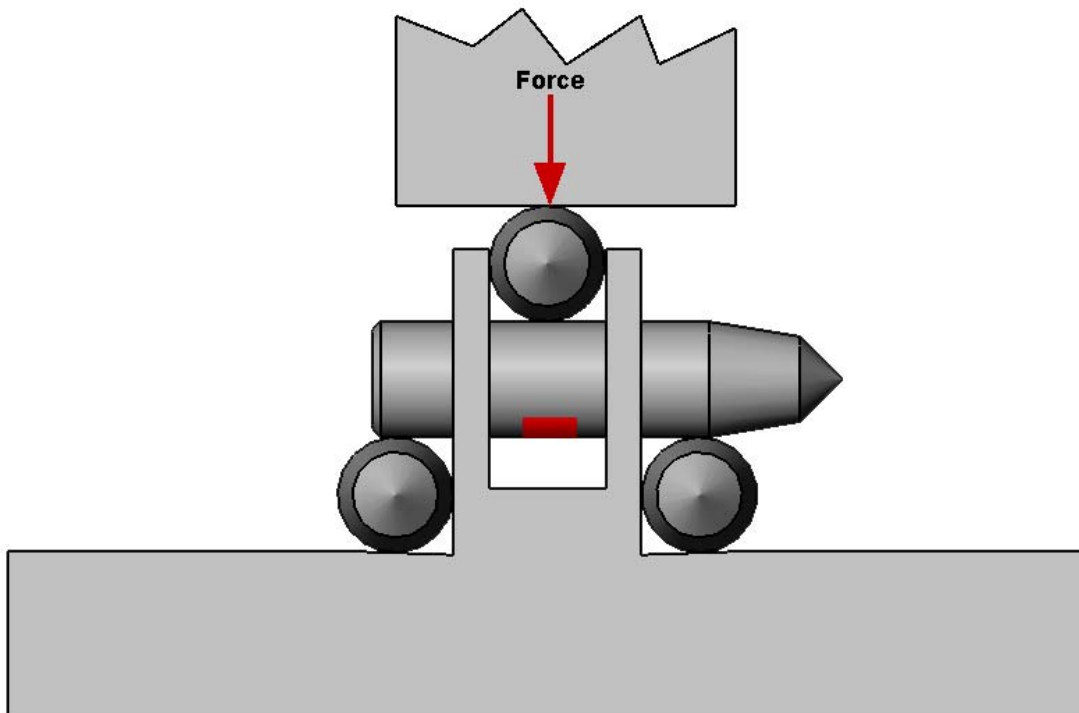

Figure 2.1: The set up of the experiment for the hardcore of 7 mm in diameter.

The experimental recordings were the force and the longitudinal and transverse strain of the cylindrical test specimen. A strain gauge was placed on the tensile side of the hard core. The strain gauge records both the longitudinal and the transverse strain.
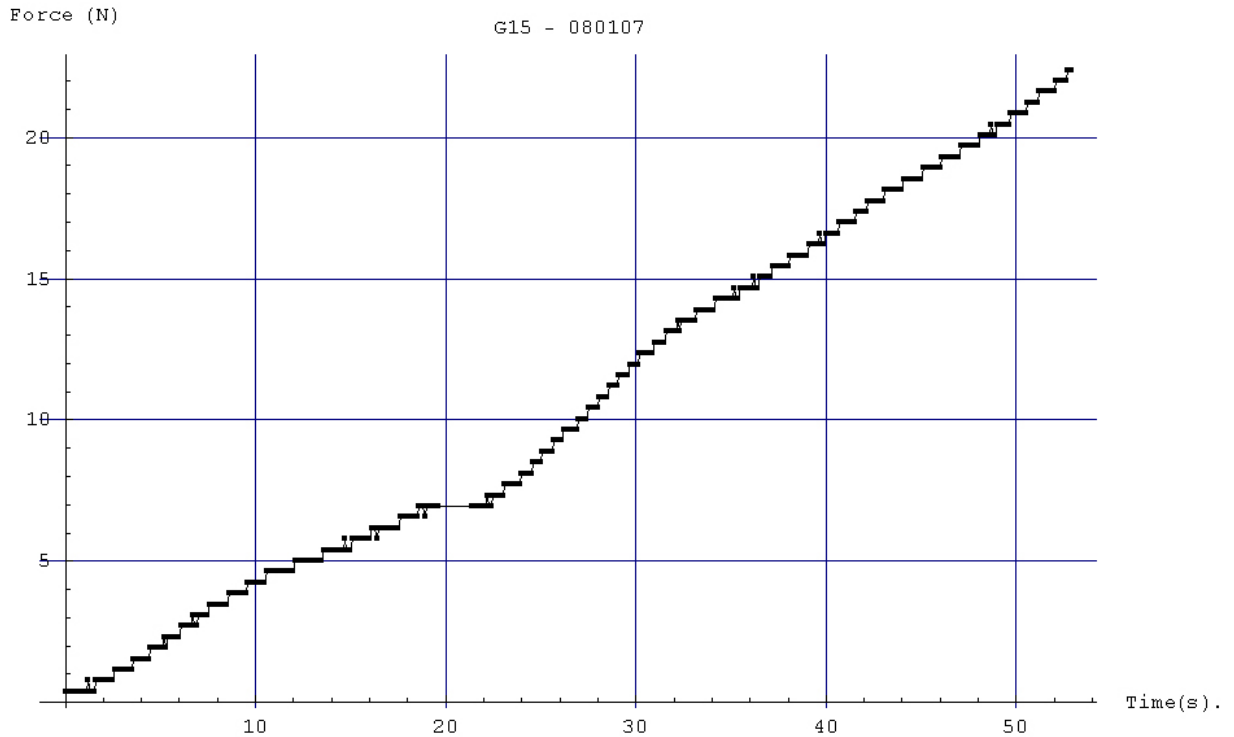
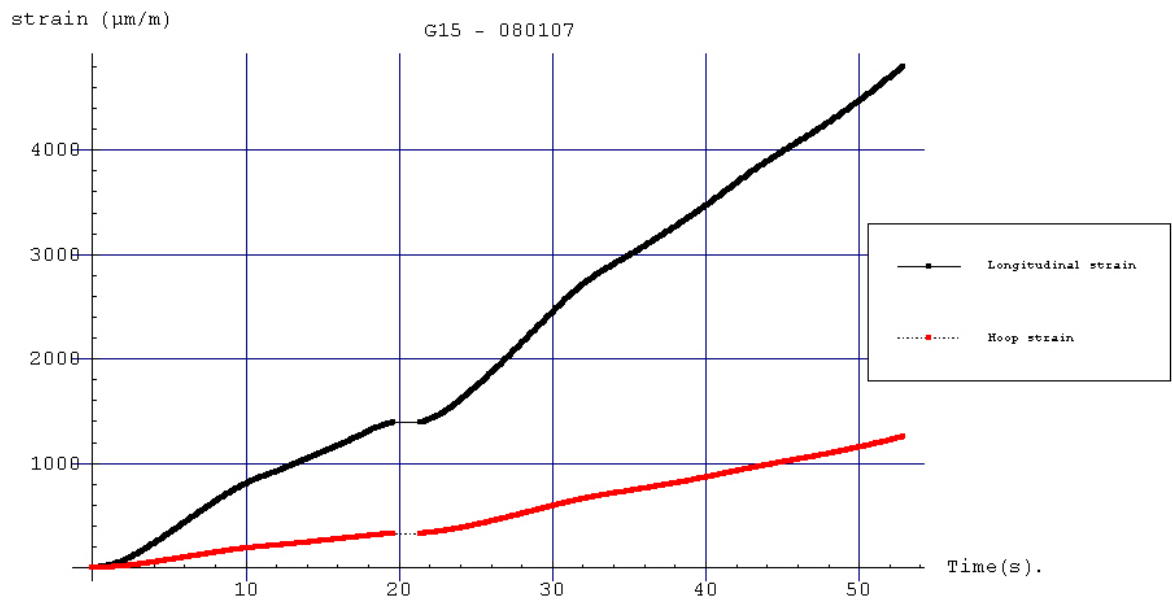*Figure 2.2: The force as a function of time during the measurement.*

Figure 2.3: The longitudinal and transverse (Hoop) strains as a function of time during the measurement.

Figures 2.2- 2.3 show typical data output from the force sensor and the two strain gauges. Figure 2.4 show a picture of the hardcore after fracturing. A good fracture is achieved if the hardcore fractures from below in a 90 degrees angle to the longitudinal axes of the hardcore.
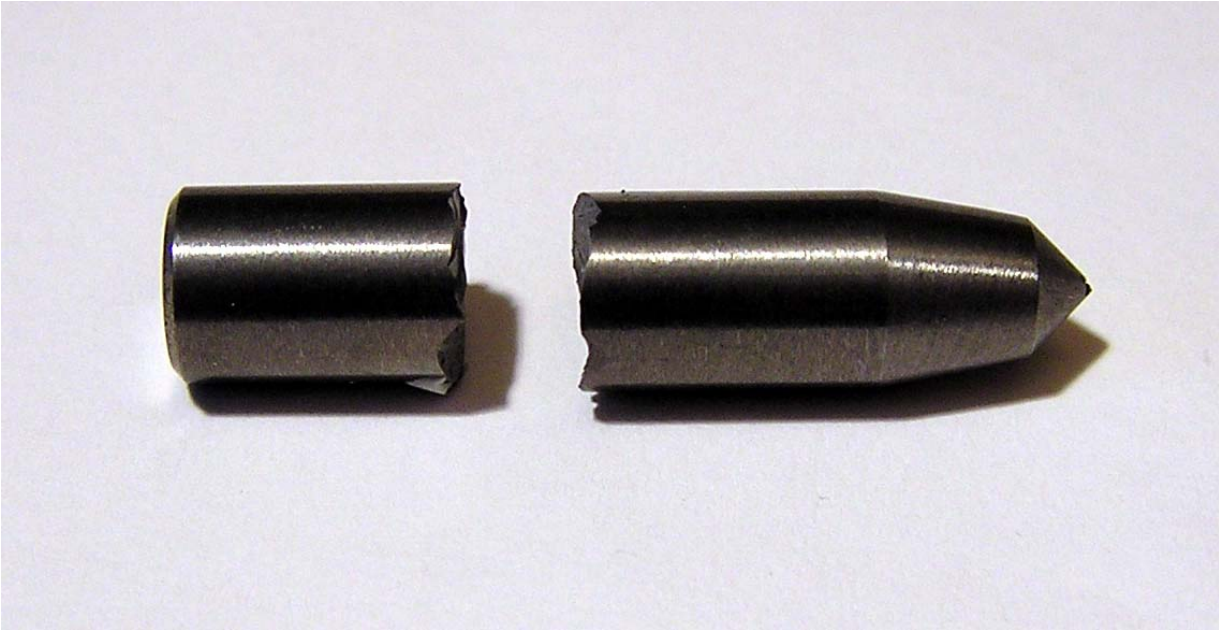
Figure 2.4: The hardmetal test specimen (d=7 mm) after fracturing due to bending

For the bending tests of the hard core with diameter of 10 mm we used several setups before we got results that were acceptable. The different set ups are shown in figures 2.5- figure 2.8. The results were, we believe, close to being not acceptable since the hardcore did not fracture in two pieces, as figure 2.9 shows.
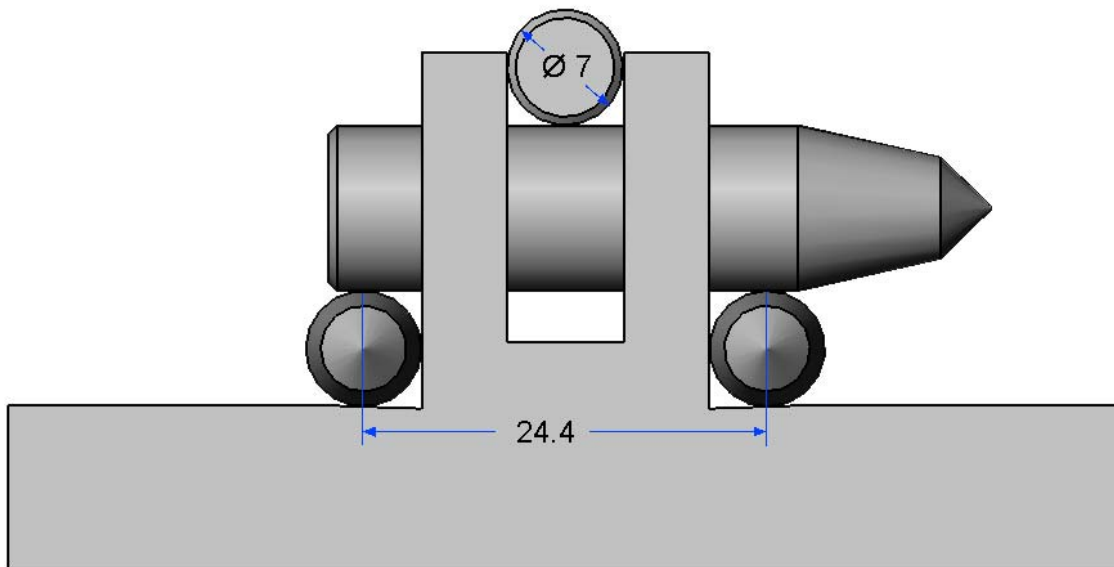

Figure 2.5: Setup alternative no. 1 for d= 10 mm hardcore.

For setup no. 1 and no. 2 the force cylinder at the top broke before the test specimen.
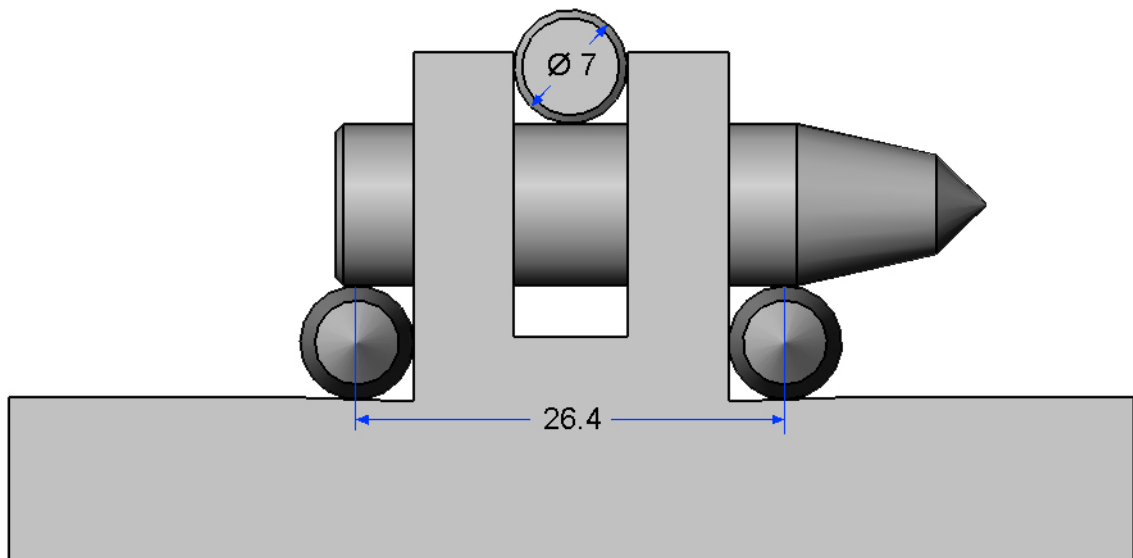
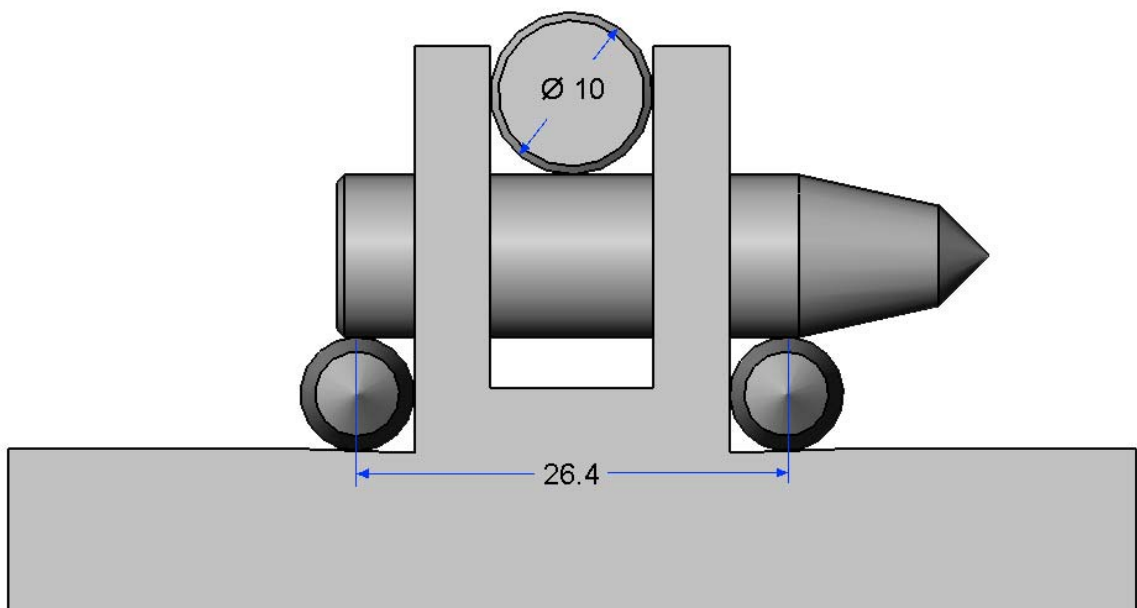*Figure 2.6: Setup alternative no. 2 for d= 10 mm hardcore.*

Figure 2.7: Setup alternative no. 3 for d= 10 mm hardcore.

For setup no. 3 the test specimen broke too early in the contact point with the left support cylinder. This was due to the too small distance from the contact point and the back of the test specimen.
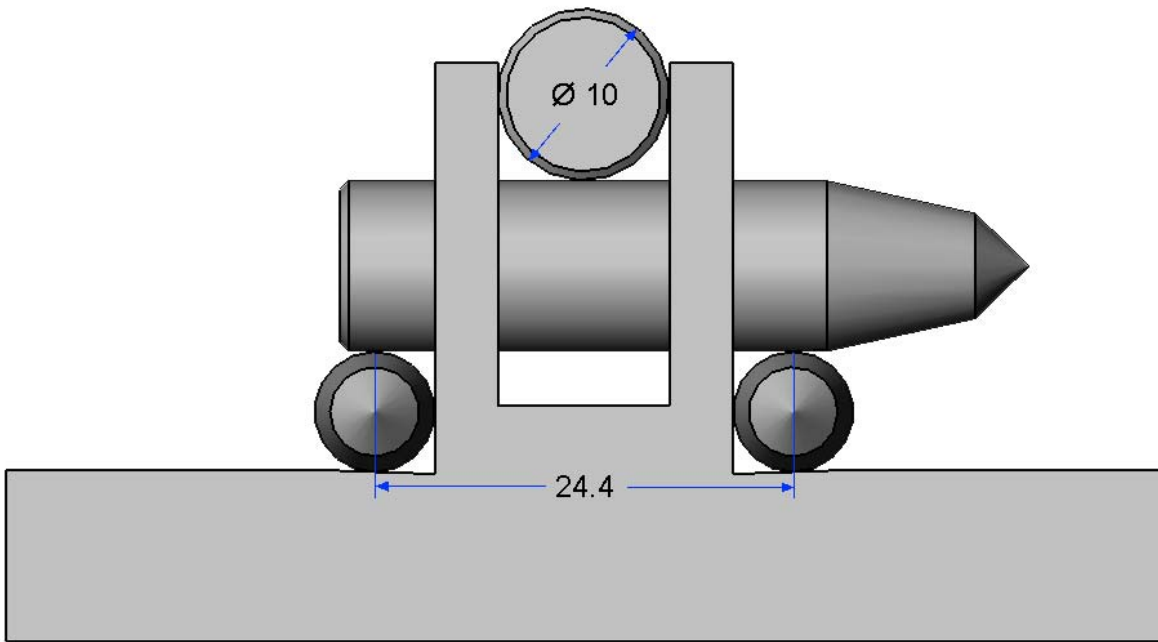
Figure 2.8: Setup alternative no. 4 for d= 10 mm hardcore. This is the setup that finally gave acceptable results.

In setup no. 4 we got acceptable results, although for some of the tests (3 out of 4) both the test specimen and the force cylinder broke at the same time.
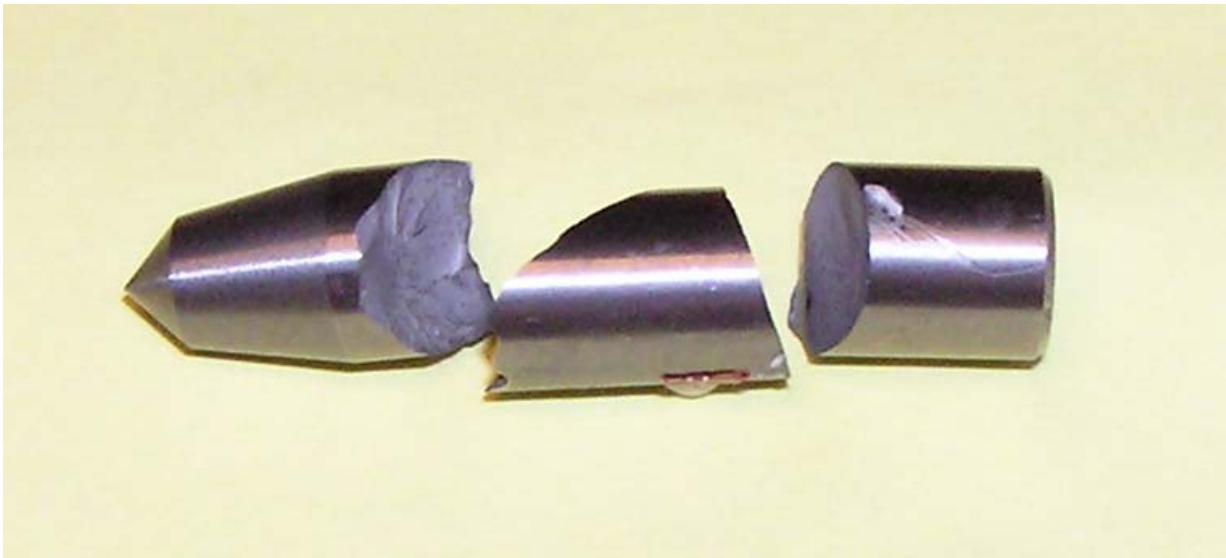

Figure 2.9: The hardcore test specimen (d=10mm) after fracture due to bending.

3 THEORY

Assume that a rod of circular cross section with length l (the distance between the supporting points of the hardcore) is bent by a force f applied to its mid-point. During bending the rod is stretched at some points and compressed at others. The neutral surface of the rod separates the region of compression from the region of tension.

The solution of the bending displacement of the neutral surface is given by $\zeta(x)$, where x is the distance along the rod. The familiar linear bending equation is

$$\zeta(x)^{(4)} \overset{mod}{=} 0, when \; x \neq l/2 \tag{3.1}$$

At $x = l/2$, ζ, ζ' and $\zeta^{(2)}$ are continuous, while the discontinuity of the shearing force, $-EI\zeta^{(3)}$, is equal to the applied force f. E is Young's modulus of the rod, and I is the principal moments of inertia. A circular rod has $I = (1/4)\pi a^4$, where a is the radius of the rod. By assuming supporting edges, i.e. $\zeta(0) = \zeta(l) = 0$, the general solution of the displacement is

$$\zeta(x) = f\,(4l^2 x - 4x^3)/(48\,E\,I), \zeta(l/2) = f\,l^3/(48\,E\,I), \quad I = (1/4)\pi a^4 \tag{3.2}$$

Observe the linearity between the force and the displacement. Also note that $E\,I\zeta^{(3)}(x) = -f/2$.

The longitudinal strain is given by

$$\varepsilon_{xx} \overset{mod}{=} z/R(x) \approx \zeta''(x)\,z \tag{3.3}$$

where z is the vertical distance from the neutral surface in the rod, and R is the radius of curvature of the specimen. According to the elastic theory we have that

$$\sigma_{xx} = \frac{E}{(1+v)(1-2v)}\big((1-v)\varepsilon_{xx} + v(\varepsilon_{yy} + \varepsilon_{zz})\big),$$

$$\sigma_{yy} = \frac{E}{(1+v)(1-2v)}\big((1-v)\varepsilon_{yy} + v(\varepsilon_{xx} + \varepsilon_{zz})\big), \tag{3.4}$$

$$\sigma_{zz} = \frac{E}{(1+v)(1-2v)}\big((1-v)\varepsilon_{zz} + v(\varepsilon_{xx} + \varepsilon_{yy})\big)$$

where v is the Poisson ratio. Assume that at the lower point a plane with normal vector in the direction of the applied force is stretched in the longitudinal and transversal direction. Assume that $\sigma_{zz} \overset{mod}{=} 0$ (the stress is in the direction of the applied force on the rod on a plane with normal vector along the direction of the applied force). From (3.4) it follows that

$$\sigma_{xx} = \frac{E}{(1-v^2)}\left(\varepsilon_{xx} + v\varepsilon_{yy}\right), \sigma_{yy} = \frac{E}{(1-v^2)}\left(\varepsilon_{yy} + v\varepsilon_{xx}\right), \sigma_{zz} = 0 \tag{3.5}$$

Inserting relation (3.3) in (3.5) and using equation (3.2) gives when letting $z = a$ and $x = l/2$, that

$$\varepsilon_{xx} = \zeta''(x)z = f\,l/(4\,E\,I), \zeta''(x) = f\,x/(2\,E\,I), (a)$$

$$\sigma_{xx} = \frac{E}{(1-v^2)}\left(\zeta''(x)\,z + v\varepsilon_{yy}\right) = \frac{E}{(1-v^2)}\left(\frac{f\,la}{4\,E\,I} + v\varepsilon_{yy}\right), (b) \tag{3.6}$$

In addition, if the state of stress is a simple tension, it follows for a linear material that $\varepsilon_{yy} = -v\varepsilon_{xx}$. Inserting this relation into (3.6) gives a more common relation, to read

$$\varepsilon_{xx} = f\,l/(4\,E\,I), \sigma_{xx} = E\varepsilon_{xx} = \frac{f\,la}{4I} \tag{3.7}$$

Observe the linearity between the stress and the force in equation (3.7). By measuring the force, the stress σ_{xx} can be calculated by using (3.7). The stress can be plotted as a function of the measured longitudinal strain ε_{xx}.

For logical reason, simply define a stress by

$$\sigma_{xx} \stackrel{def}{=} \frac{E}{(1-v^2)}\left(\varepsilon_{xx} + v\,\varepsilon_{yy}\right), \tag{3.8}$$

We will first check whether we have a state of simple tension during the bending, to read

$$\varepsilon_{yy} = -v\,\varepsilon_{xx}, ? \tag{3.9}$$

This relation is checked by using the measured longitudinal and transverse strain from this study together with the Poisson ratio found from earlier compression tests. Both the measured longitudinal and transverse strain can be inserted into equation (3.8). If relation (3.9) holds we simply achieve $\sigma_{xx} = E\varepsilon_{xx}$. Thus we can indirectly check whether (3.9) holds by checking whether $\sigma_{xx} = E\varepsilon_{xx}$. This will be our approach, i.e. we insert the longitudinal and transversal strain into equation (2.8) and plot the stress as a function of the longitudinal strain. We compare the result with the curve $\sigma_{xx} = E\varepsilon_{xx}$. E is given from the literature or from earlier studies.

Next we will check whether the relations in (3.1) and equation (3.3) holds, or whether $\sigma_{zz}^{mod} = 0$ is fulfilled. The equations can be summarized to (3.6a), i.e.

$$\varepsilon_{xx} = f\,l/(4\,E\,I), ? \Rightarrow f\,l/(4\,I) = E\varepsilon_{xx}\,? \tag{3.10}$$

Thus our approach is to plot $f\,l/(4\,I)$ towards ε_{xx} and to check whether the steepness of the curve is dependent of the size of the hardcore.

Finally we record the longitudinal stress and strain at fracture.

4   RESULTS

In this section we give the results for different types of hard cores. The diameters of the hardcores are d= 7 mm and d= 10 mm.
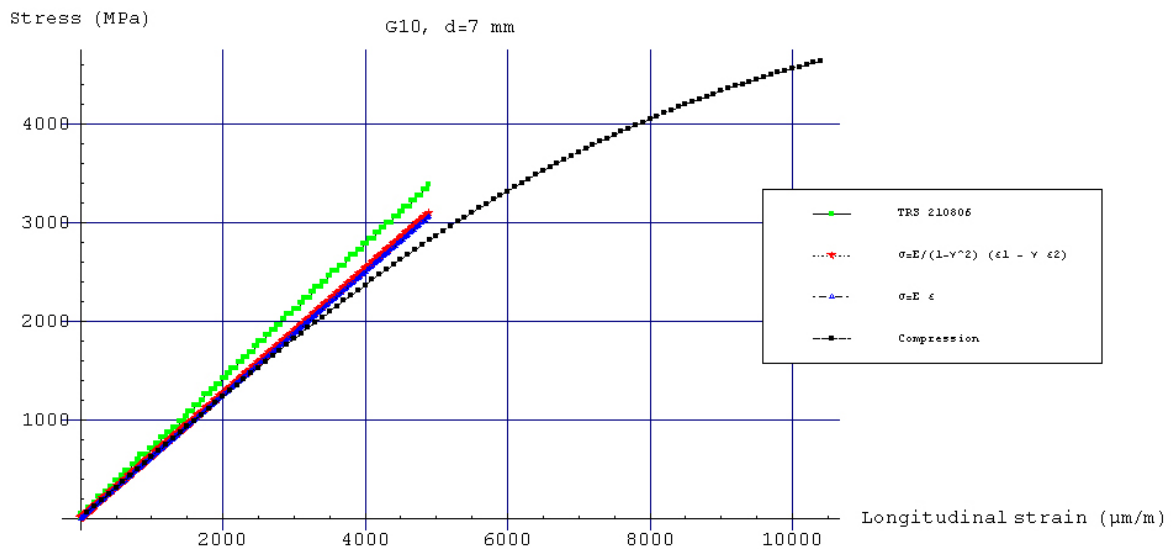
4.1   G10, d=7 mm

Figure 4.1: The simple tension and simple compression experiment for G10, 7 mm in diameter.

Figure 4.1 gives the results from an earlier compression test and the tensile test in this report. Four different curves are plotted. The dark curve is the compression curve found in earlier studies. The close agreement between the red and the blue curve shows that we have to a good approximation a state of simple tension. The discrepancy between the green curve and the red/ blue could mean that the measured force does not lead the longitudinal stress when using our formula. Thus some of the assumptions

$$\zeta(x)^{(4)} \overset{mod}{=} 0, when \ x \neq l/2 \ , \varepsilon_{xx} \overset{mod}{=} \ z/R(x) \approx \zeta^{"}(x)\,z, \sigma_{zz} \overset{mod}{=} \ 0 \ \text{in the theory could we too}$$

rough, but we will show that the most reasonable assumption is that the hardcore has a larger Young's modulus in tension than in compression. Also observe that the relationship between the measured force (stress) and measured strain is linear. The stress versus strain curve simply does not follow the compression curve in the non-linear region. Figure 4.2 shows the results for two different hardcores of G10. The stress is calculated by using the measured force.

Figure 4.3 shows the result the average together with the standard deviation. The average fracture point is also shown. Figures 4.4 – 4.6 show the results for the KMS hardcore. Three different hardcores were used. Compared to G15 we find a somewhat larger spread of the fracture point.
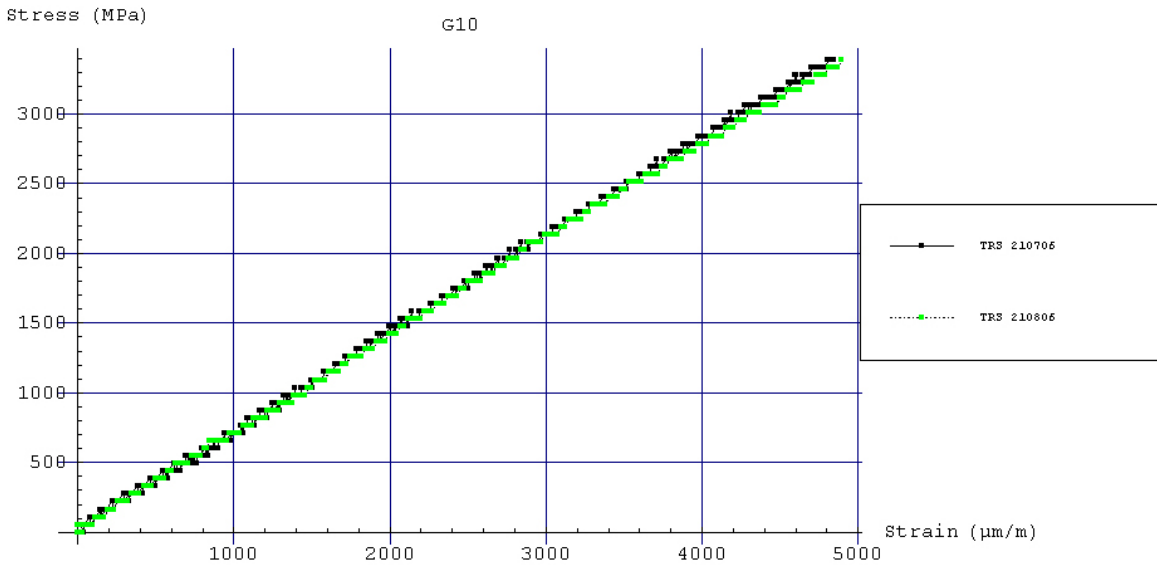

Figure 4.2: The stress as a function of strain for the two runs for G10.
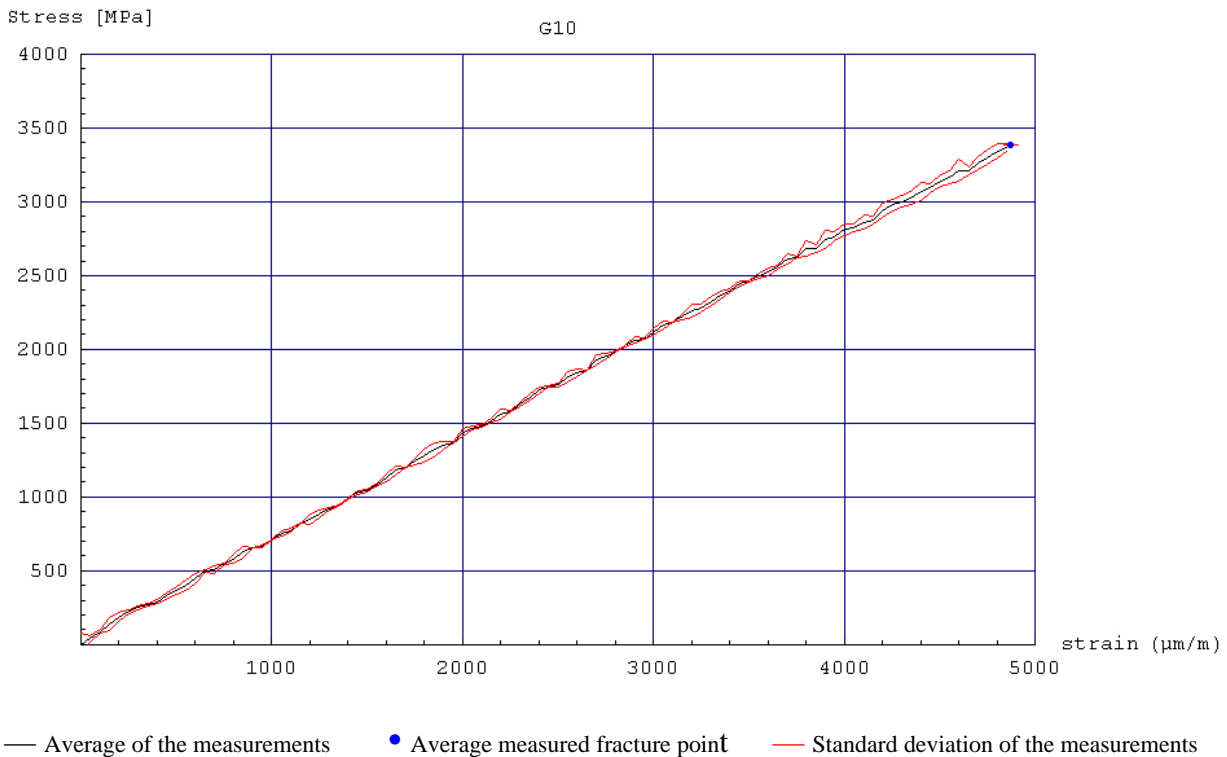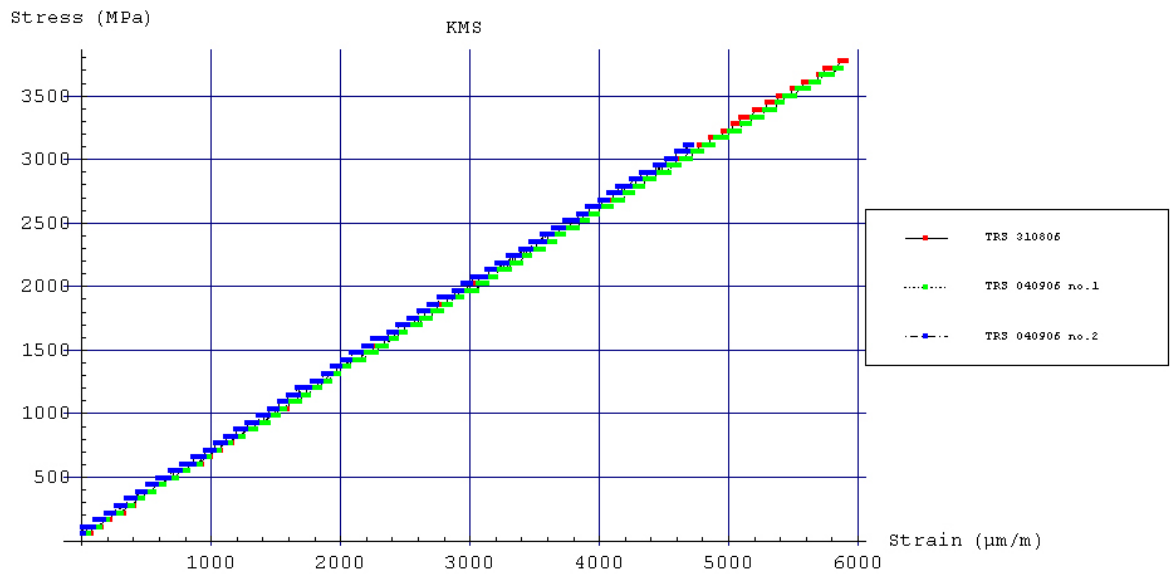

—— Average of the measurements   • Average measured fracture point   — Standard deviation of the measurements

Figure 4.3: The stress as a function of strain. Average curve together with the standard deviations and fracture point for G10.

4.2   KMS, d=7 mm
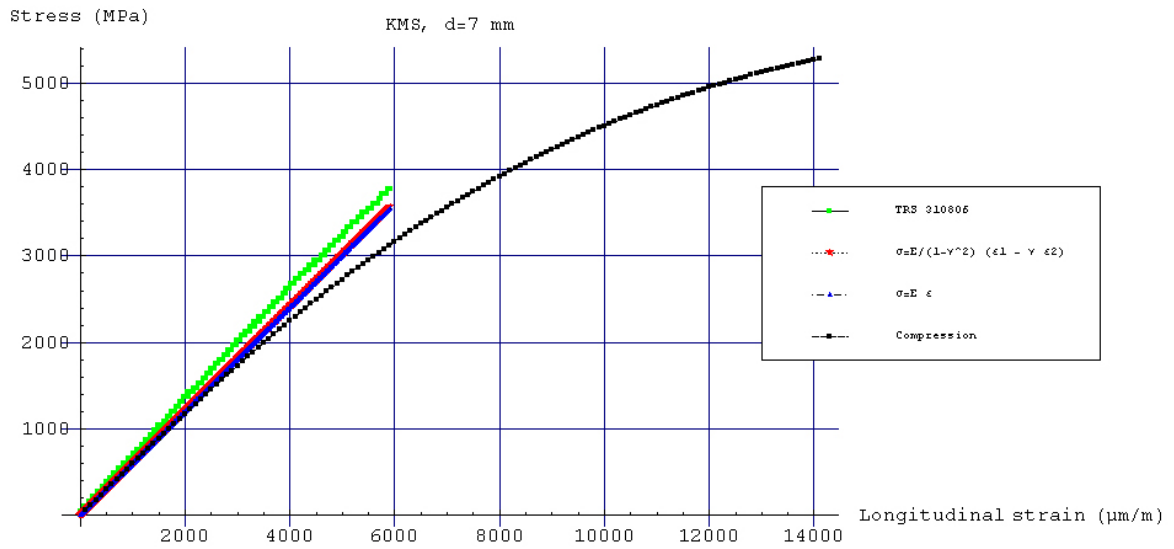
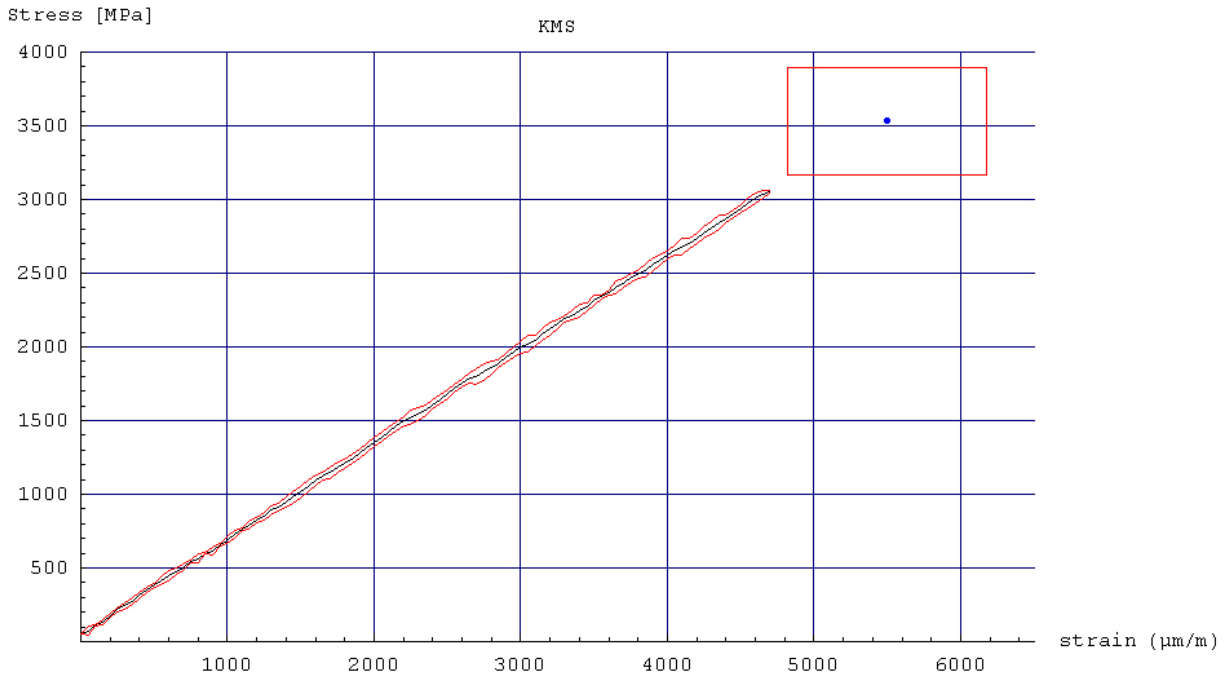*Figure 4.4: The simple tension and simple compression results for KMS, 7 mm in diameter.*

Figure 4.5: The stress as a function of strain for the three runs for KMS.

— Average of the measurements   • Average measured fracture point   — Standard deviation of the measurements

Figure 4.6: The stress as a function of strain. Average curve together with the standard deviations and fracture point for KMS.
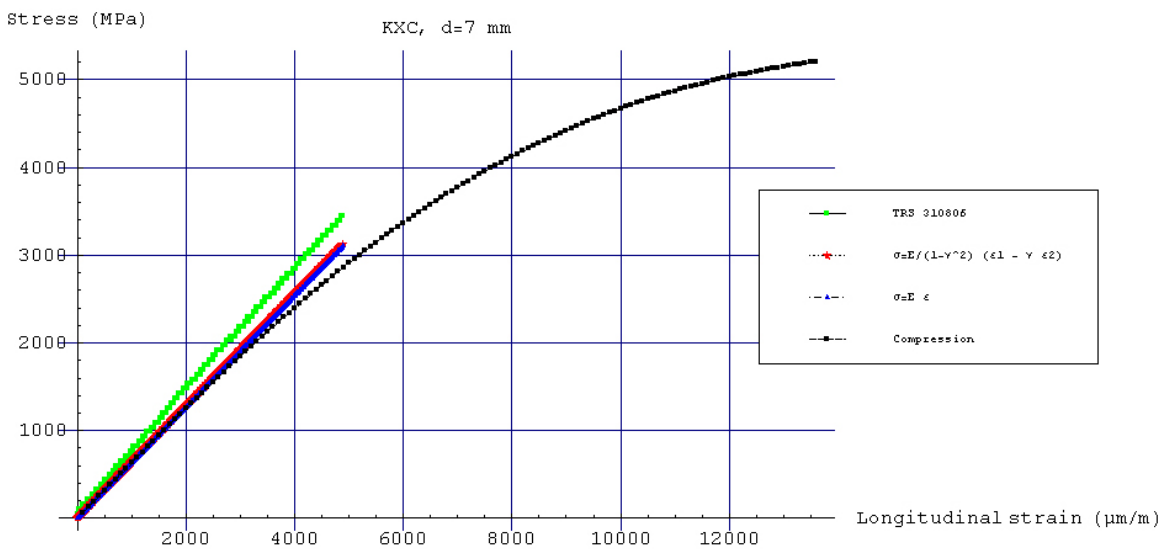
4.3   KXC, d=7 mm

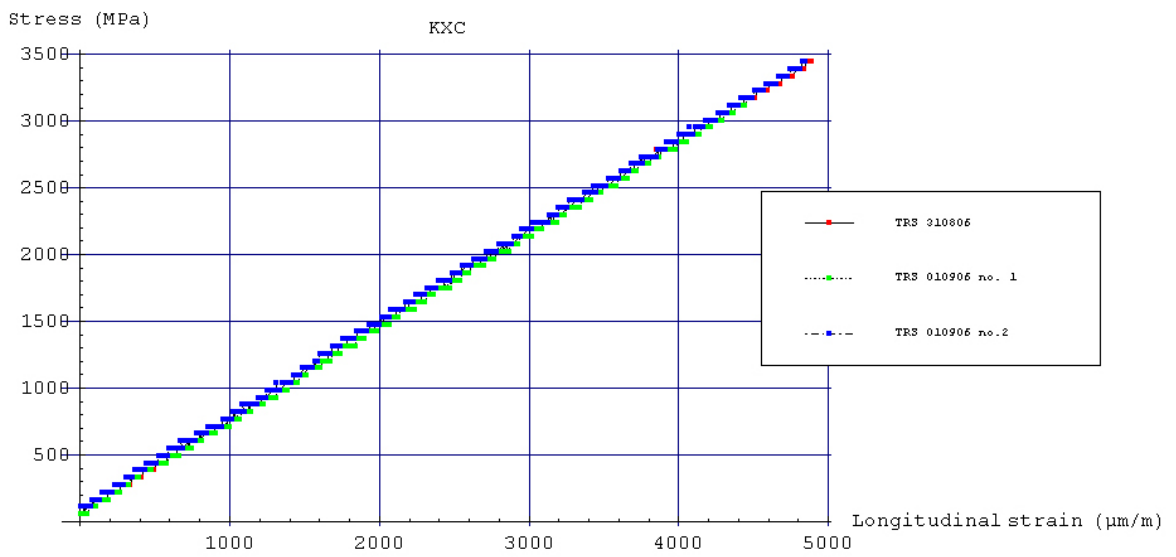*Figure 4.7: The simple tension and simple compression results for KXC, 7 mm in diameter.*

Figure 4.8: The three runs for KXC.

—— Average of the measurements　　● Average measured fracture point　　—— Standard deviation of the measurements
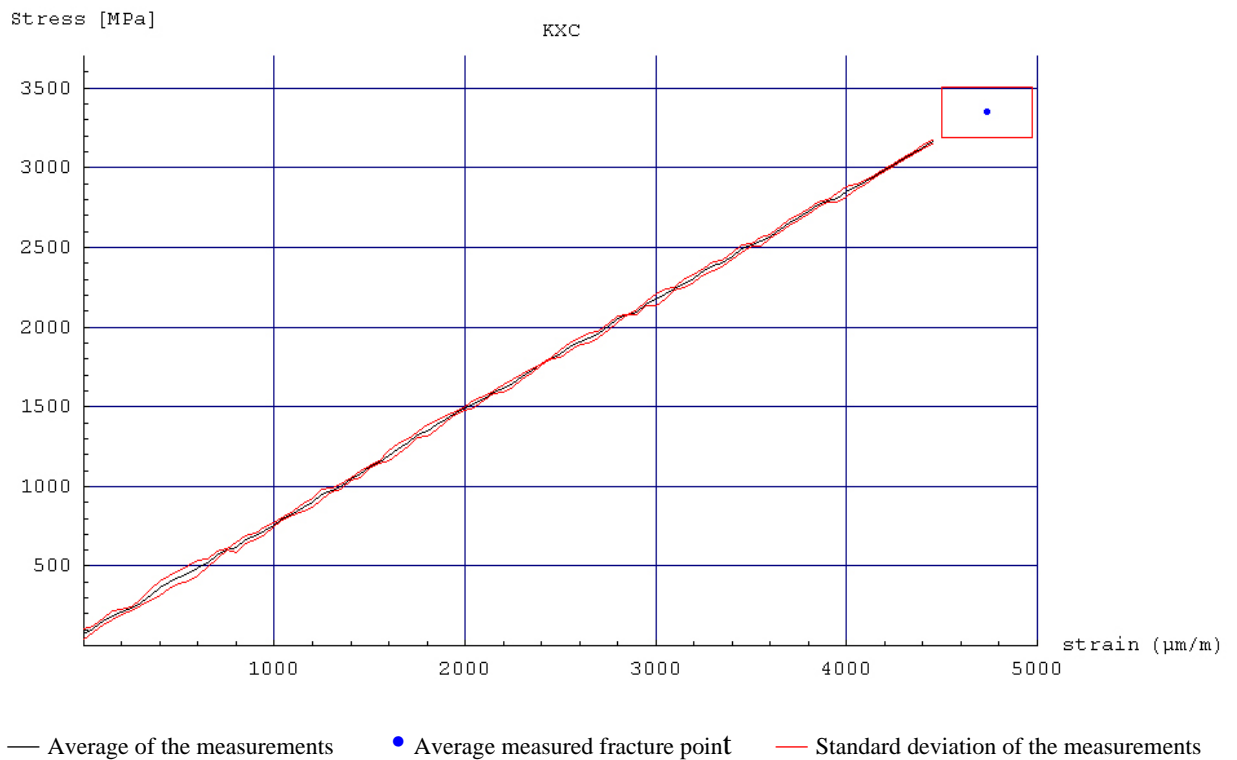
Figure 4.9: Average curve and break point for KXC.
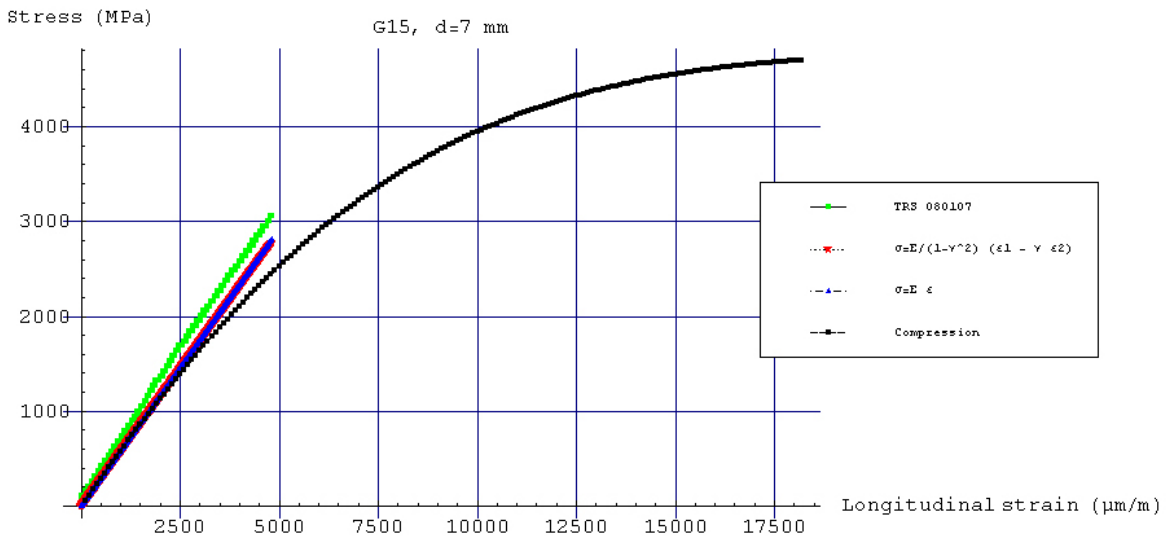
4.4   G15, d=7 mm

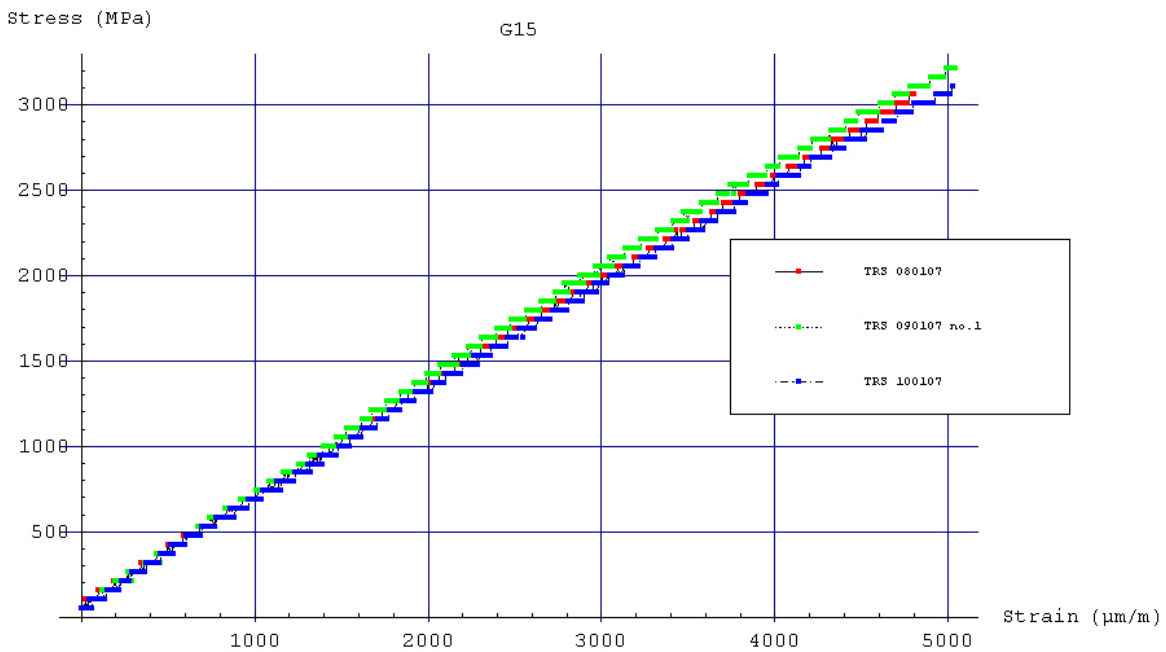*Figure 4.10: The simple tension and simple compression results for G15, 7 mm in diameter.*
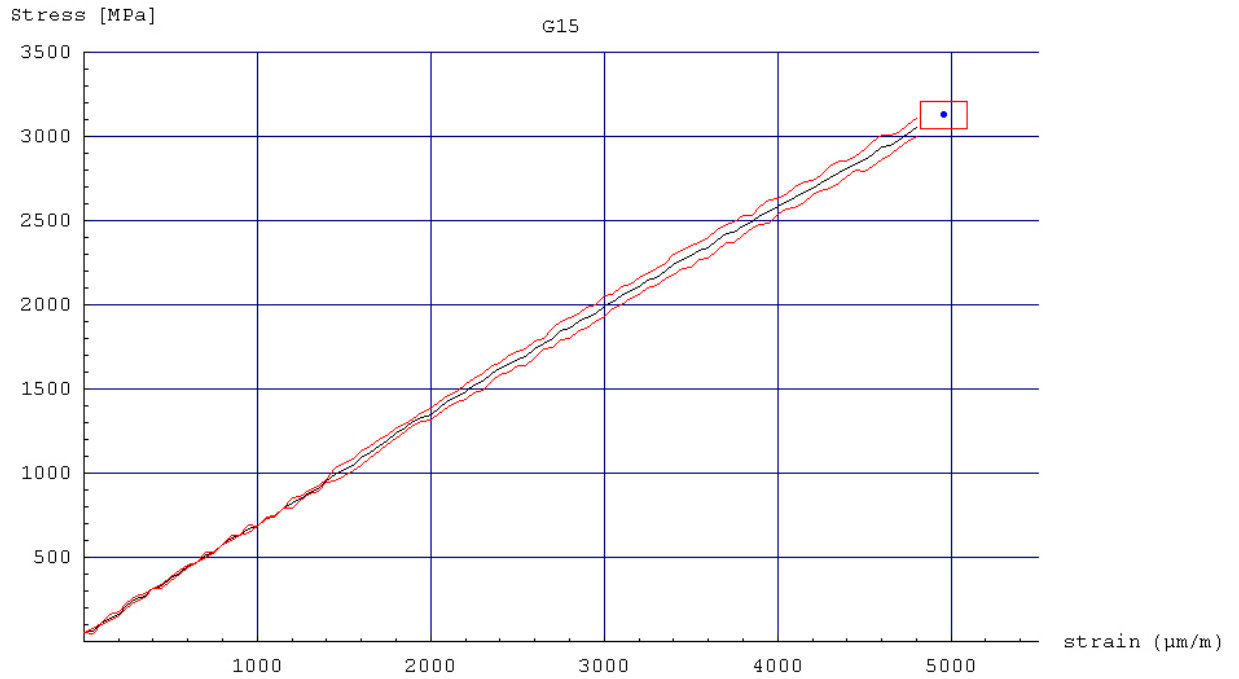

Figure 4.11: The three runs for G15.

—— Average of the measurements   ● Average measured fracture point   —— Standard deviation of the measurements

Figure 4.12: Average curve and fracture point for G15, 7 mm in diameter.

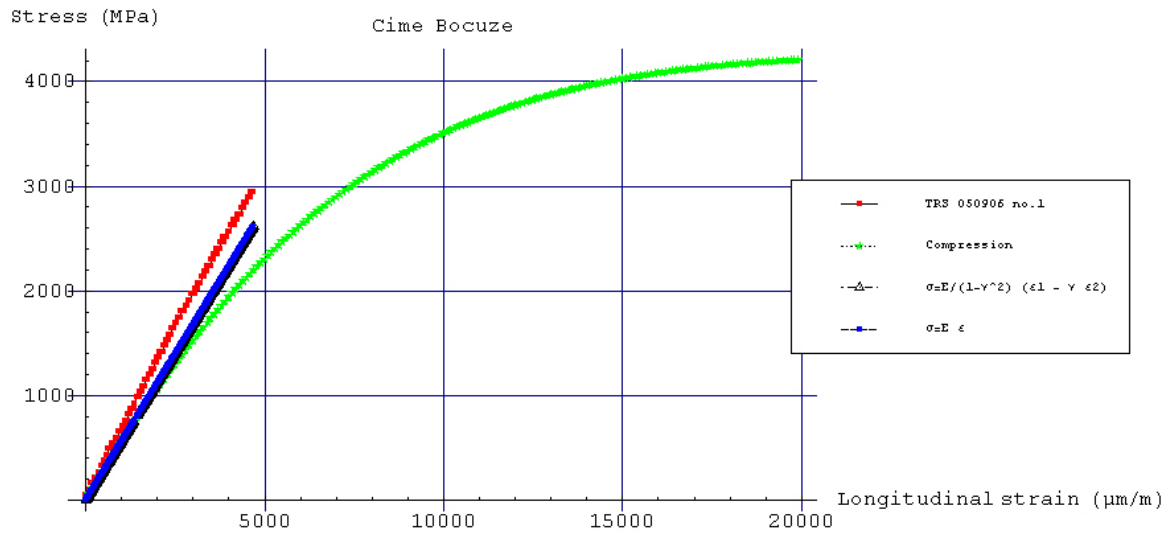## 4.5   Cime Bocuze, d=7 mm (Job number: 13900005, Manufacturing source: 945922)

Figure 4.13: The simple tension and simple compression results for Cime Bocuze, 7 mm in diameter.
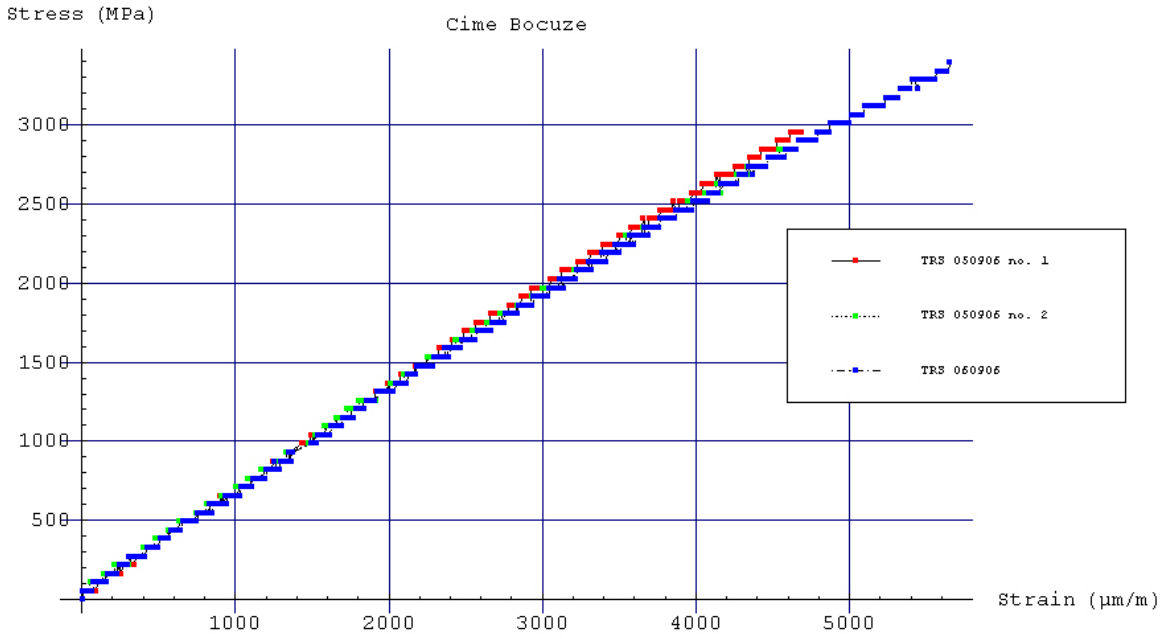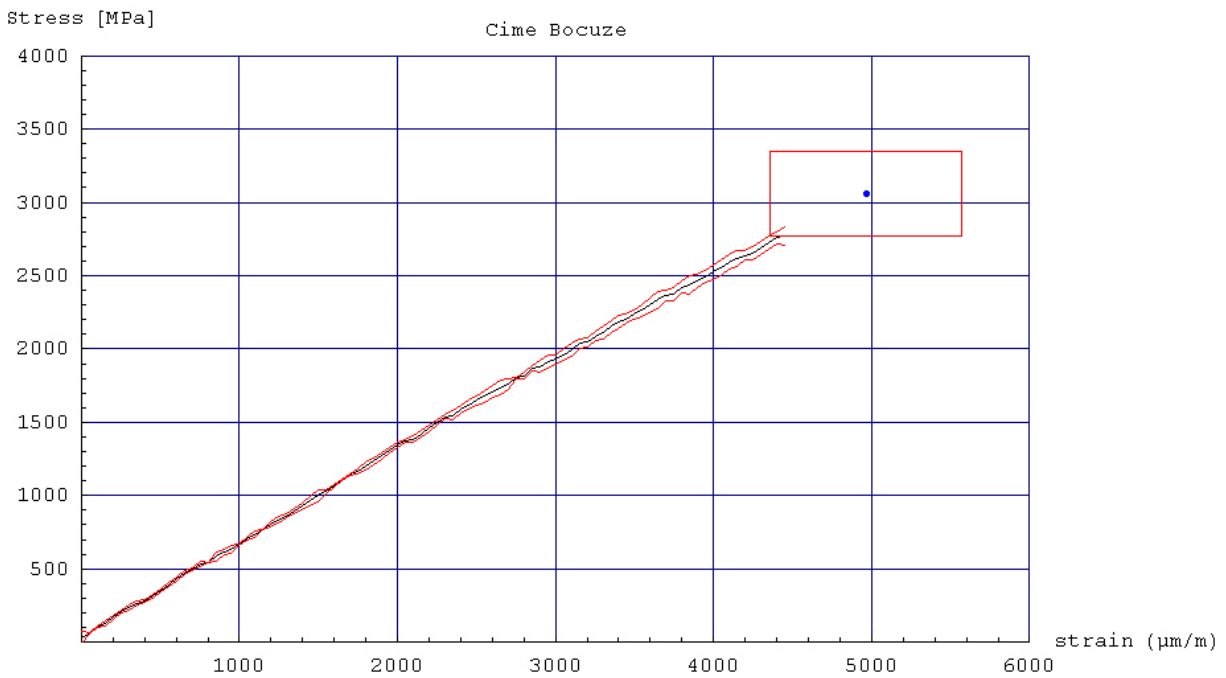
Figure 4.14: The three runs for Cime Bocuze.

— Average of the measurements   ● Average measured fracture point   — Standard deviation of the measurements

Figure 4.15: Average curve and fracture point for Cime Bocuze , 7 mm in diameter.

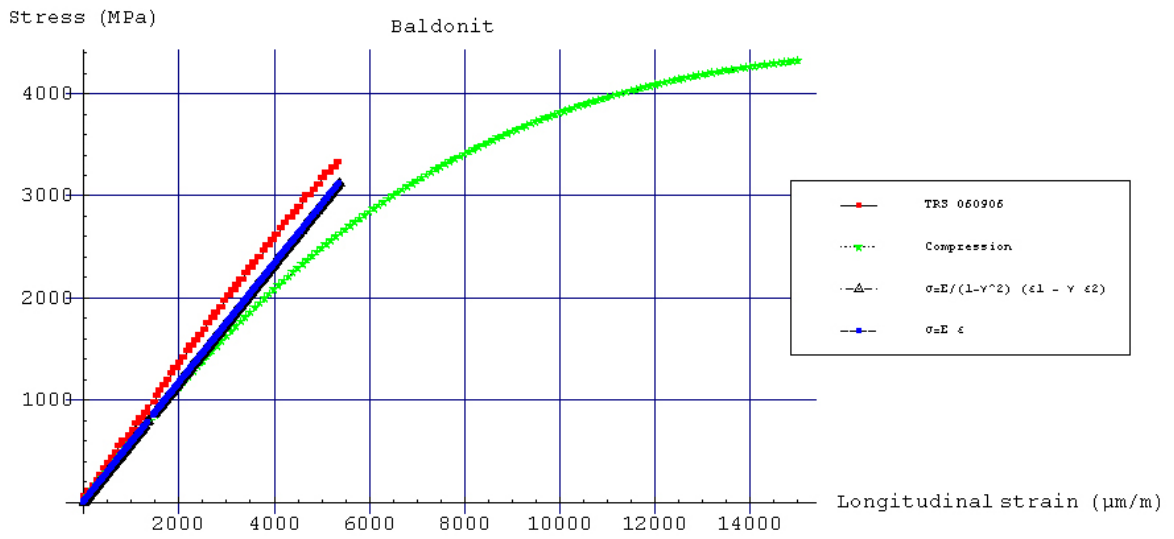## 4.6 Baldonit, d=7 mm (Lot 84, unit no. 24)

Figure 4.16: The simple tension and simple compression results for Baldonit, 7 mm in diameter.
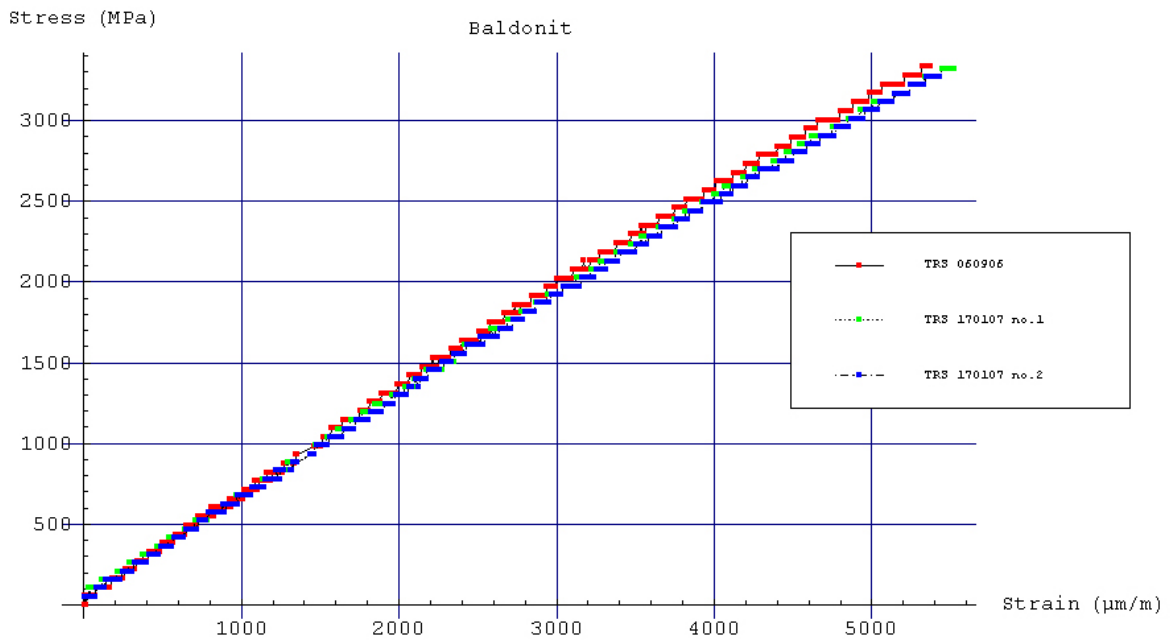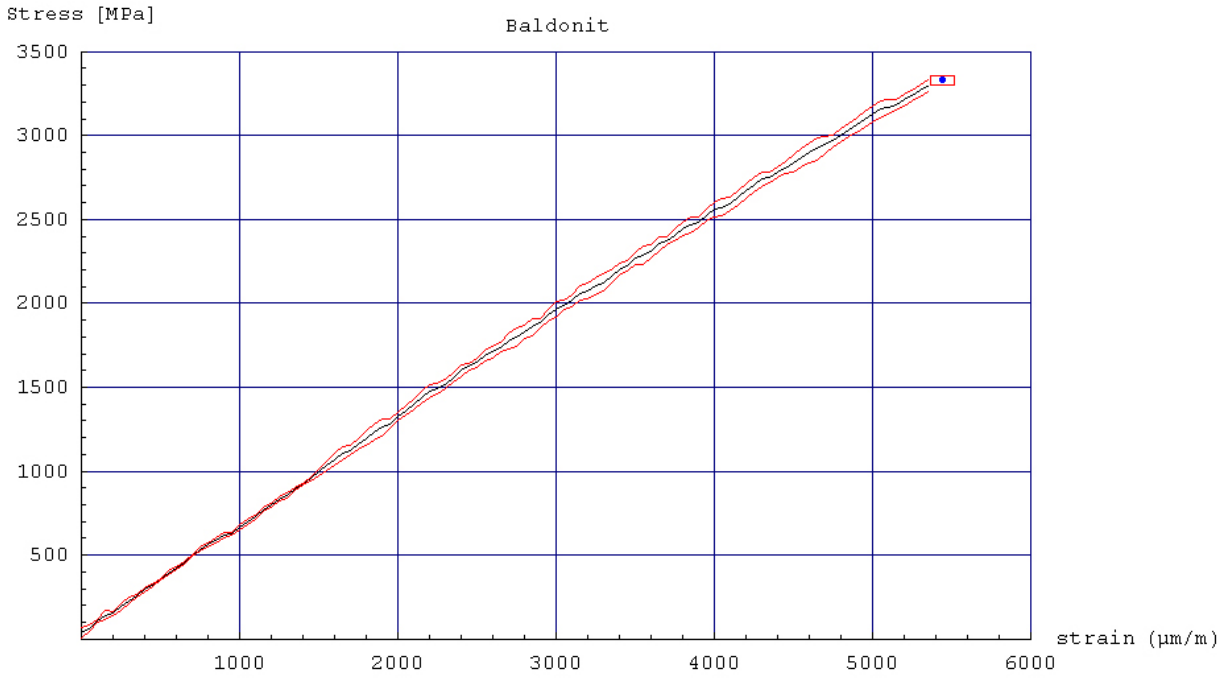

Figure 4.17: The three runs for Baldonit.

—— Average of the measurements   • Average measured fracture point   —— Standard deviation of the measurements

Figure 4.18: Average curve and fracture point for Baldonit , 7 mm in diameter.
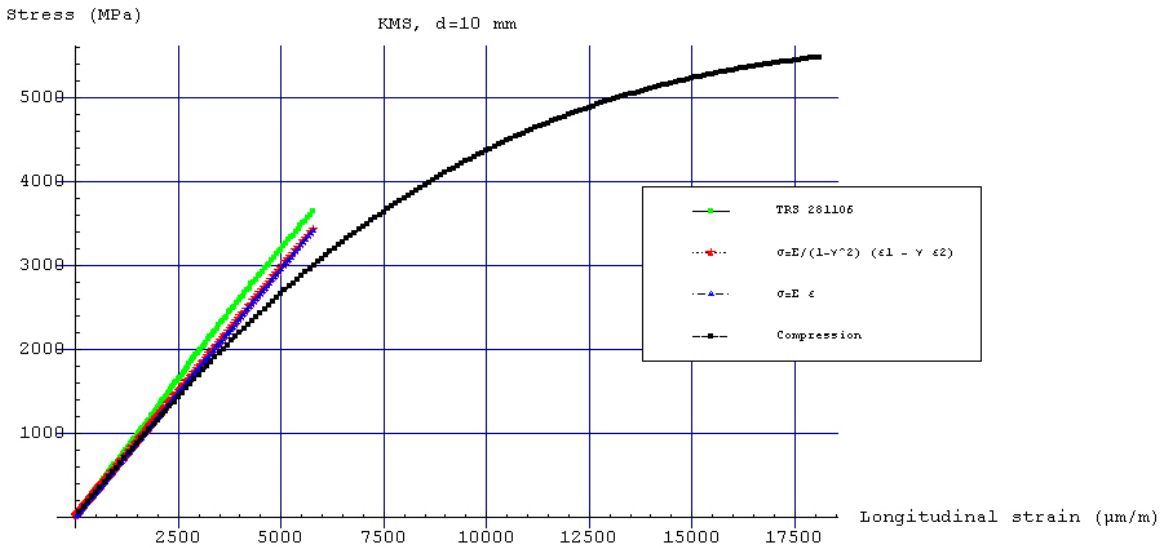
4.7   KMS, d=10 mm

Figure 4.19: The simple tension and simple compression results for KMS, 10 mm in diameter, 1 run.

4.8 KXC, d=10 mm
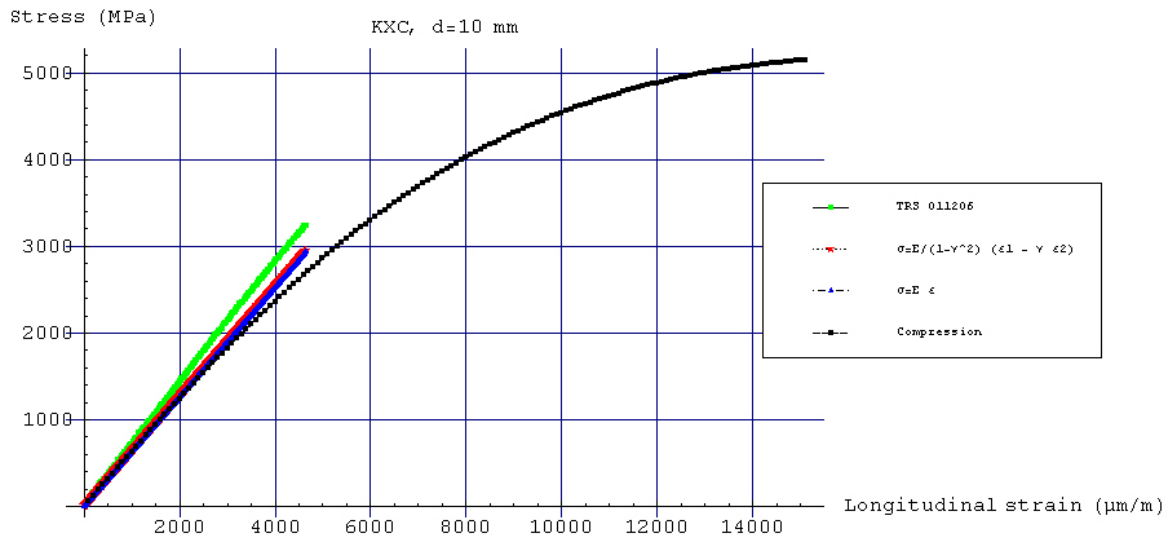
Figure 4.20: The simple tension and simple compression results KMS, 10 mm in diameter, 1 run.

4.9 KF1, d=10 mm

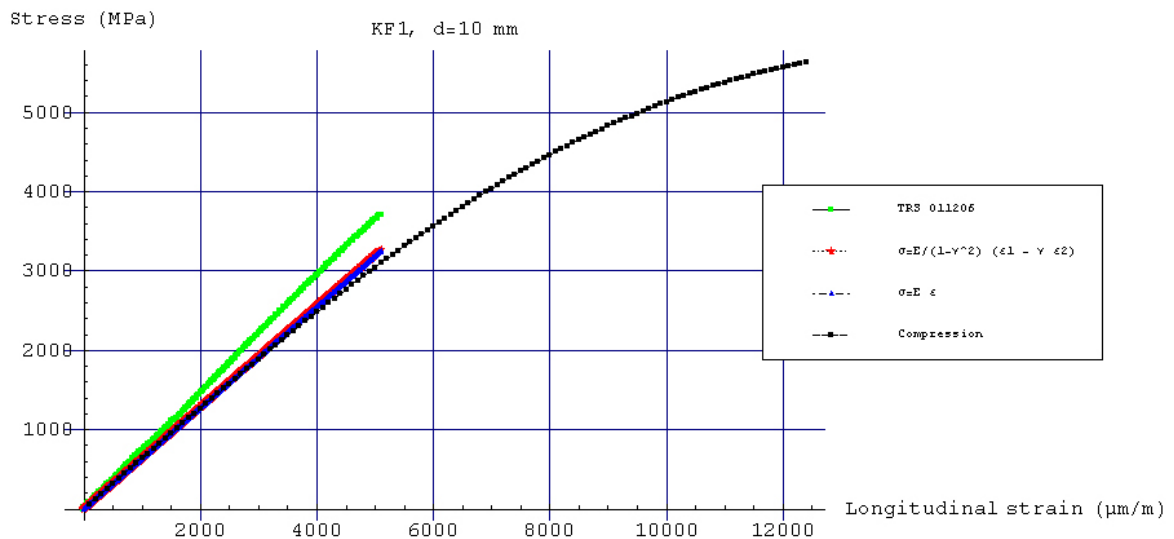*Figure 4.21: The simple tension and simple compression results for KF1, 10 mm in diameter.*
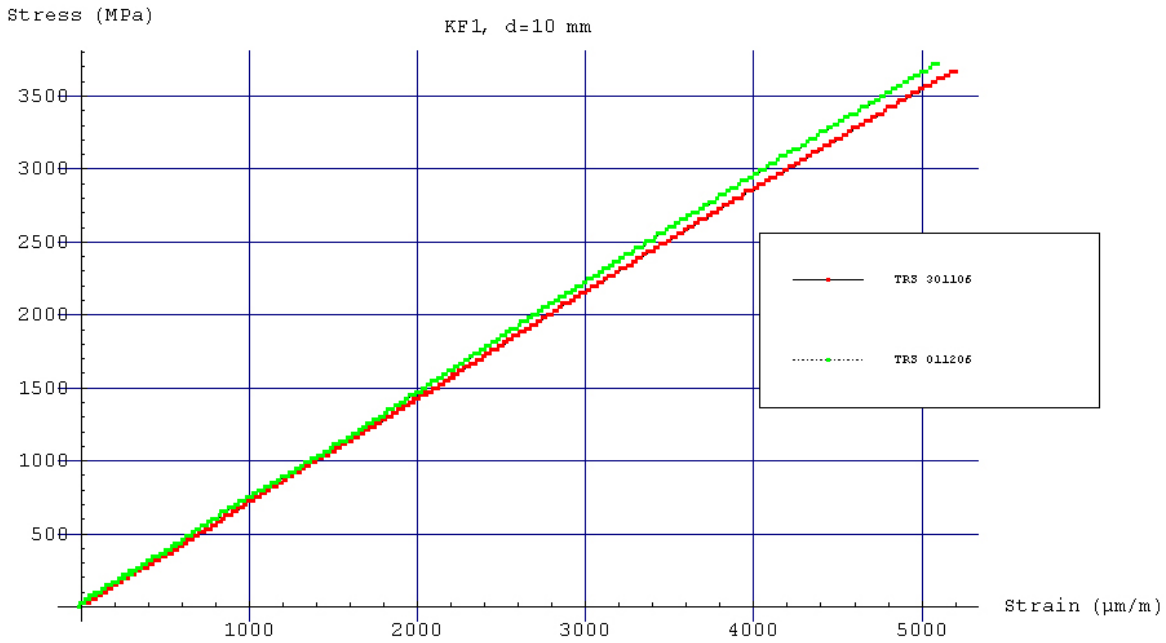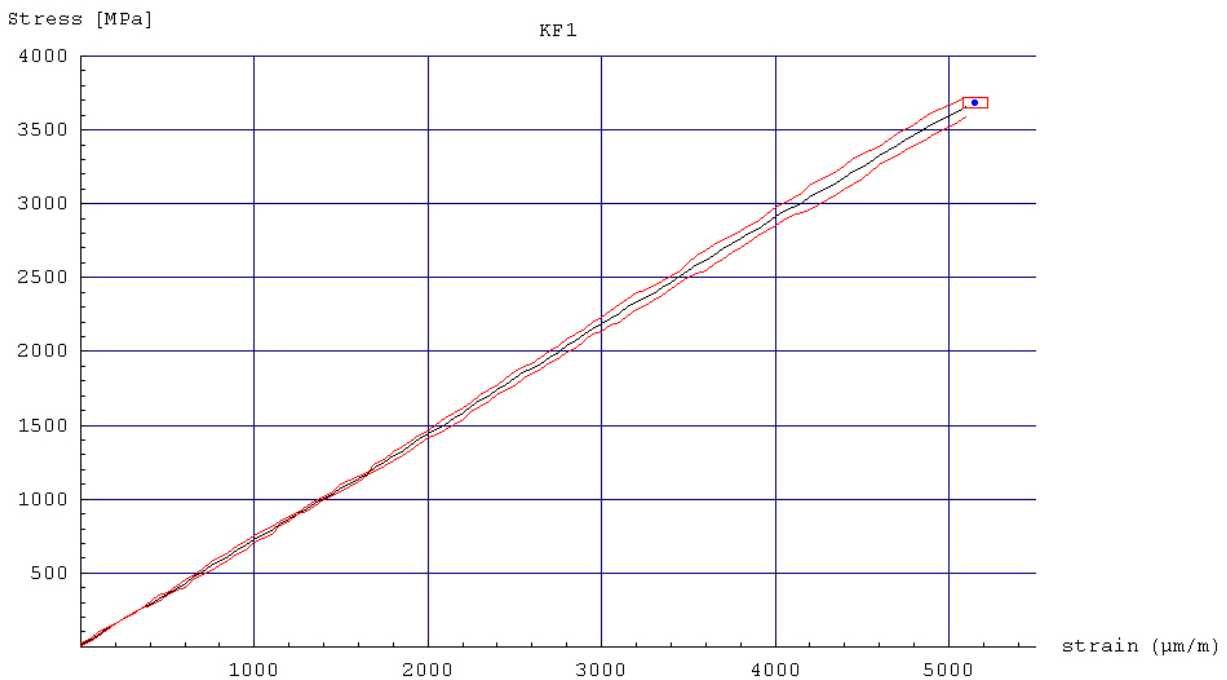
Figure 4.22: The two runs for KF1.

—— Average of the measurements   • Average measured fracture point   — Standard deviation of the measurements

Figure 4.23: Average curve and fracture point for KF1.

In general the same type of behaviour is shown for all types of hardcores and for the different diameters.

5   COMPARISON OF THE STRESS-STRAIN CURVES FOR HARDCORES OF DIFFERENT DIAMETERS

As shown in the previous section, using the measured force for stress calculations give some deviations when compared to the compression curve. We anticipated a larger Young's modulus in tension than in compression. To study this more closely we compared the stresses for hardcores of diameters of 7 and 10 mm of the same type. It is reason to believe than any bad approximations in the bending theory, or experimental errors, should lead to discrepancies between the results for the 7 mm and 10 mm hardcores since the term l/I in the force formulae is significantly different for the two sizes of hardcores. Figure 5.1 and figure 5.2 give the results for the 7 mm and 10 mm hardcores for the hardcores which were available in the two sizes. The curves for the 7 mm and 10 mm diameters match. The equality of the different sizes suggests that the bending theory is viable and that the discrepancies between the tension and compression curves are due to the material properties of the hardcore. The Young's modulus in tension is simply larger than in compression. Also the modulus is almost constant in tension.

5.1   KMS, d=7 mm vs. d=10 mm
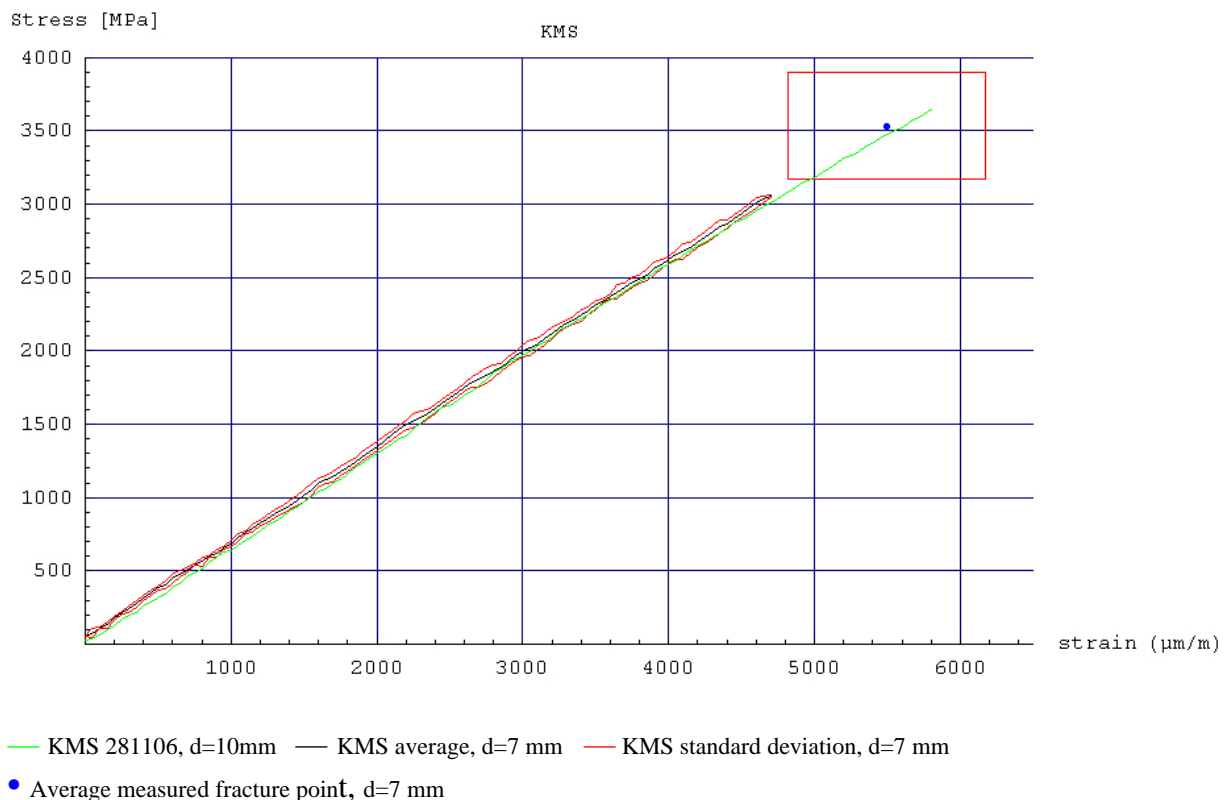

—— KMS 281106, d=10mm   —— KMS average, d=7 mm   —— KMS standard deviation, d=7 mm

● Average measured fracture point, d=7 mm

Figure 5.1: Comparison of the results from the bending experiment for KMS, 7 and 10 mm in diameter.
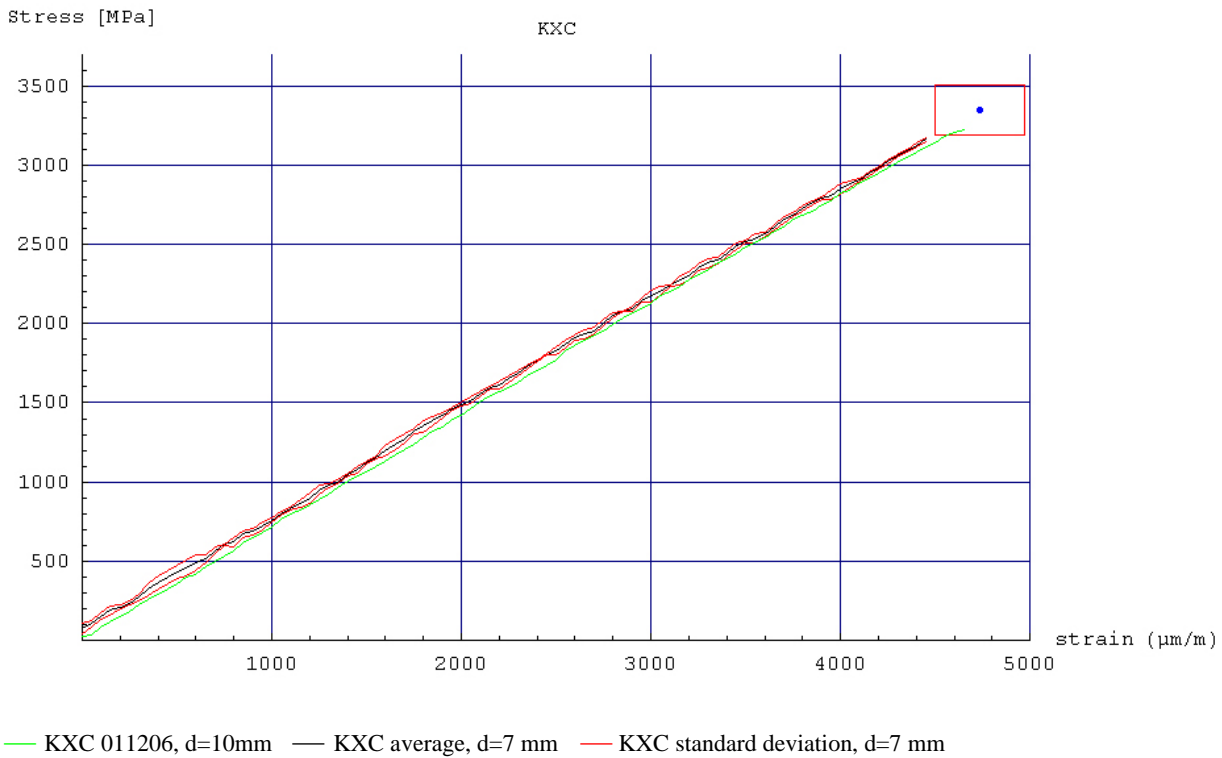
5.2 KXC, d=7 mm vs. d=10 mm

Figure 5.2: Comparison of the results from the bending experiment for KXC, 7 and 10 mm in diameter.

6 CONCLUSION/DISCUSSION

In this report an experimental study of the tensile strength of different hard cores of Wolfram Carbide was performed. A new experimental bending test was constructed for the study. We showed by comparing the measured longitudinal and transverse strain, that assuming a state of simple tension at the lower surface of the hardcore during bending is a good approximation. We find that the hardcores of different sizes have the same mechanical properties. The tensile strength and strain is much smaller than the compressive strength and strain.

We finally find a somewhat larger Young's modulus in tension than in compression. The tensile stress as a function of the strain somewhat follows the compression curve in the linear compressive stress-strain region. The lack of non-linearity compared to the compressive situation we believe is related to the mechanical properties of Cobalt that acts as glue for the Wolfram Carbide particles that constitute the hardcore.

References

1: Moxnes John F. and Frøyland Øyvind, " Mechanical studies of wolfram carbide", FFI Report, - 2004/03860
2: Moxnes John F. and Frøyland Øyvind, " Simple compression studies of wolfram carbide", FFI Report, 2006/01922

3: ISO-Standard 3327-1982, 2nd edition, "Hardmetals – Determination of transverse rupture strength"
4: Morrell R., "Flexural strength testing of ceramics and hardmetals", Measurement Good Practice Guide No. 7, National Physical Laboratory, 1997

Appendix A

| | Average fracture point | | | | | | |
	G15 (d=7 mm)	KMS (d=7 mm)	KXC (d=7 mm)	G10 (d=7 mm)	KMS (d=10mm)	KXC (d=10 mm)	KF1 (d=10 mm)
Fracture strength [MPa]	3128	3533	3351	3388	3664	3230	3689
Fracture strength std. dev. [MPa]	80	363	158	0	-	-	35
Fracture strain [μm/m]	4955	5499	4734	4872	5828	4650	5152
Fracture strain std. dev. [μm/m]	134	677	237	36	-	-	72

Table A1: The measured fracture stresses and strains during bending.

	Young's modulus tension [GPa]	Young's modulus compression [GPa]
KMS, d=7 mm	642.911	600.971
KMS d=10 mm	642.497	590.155
KXC, d=7 mm	689.583	634.632
KXC, d=10 mm	707.019	631.913
G15, d=7 mm	645.789	584.536
G10, d=7 mm	687.522	625.768
KF1, d=10 mm	712.908	637.335
Cime Bocuze, d=7 mm	634.607	558.617
Baldonit, d=7 mm	629.284	581.745

Table A2: Young's modulus in tension and compression.